# Efficient suspension plasma spray fabrication of black titanium dioxide coatings with visible light absorption performances

Mengjiao Zhai[a], Yi Liu[a], Jing Huang[a], Yingquan Wang[b], Kuan Chen[a], Yaoyao Fu[a], Hua Li[a,*]

[a] Key laboratory of Marine Materials and Related Technologies, Zhejiang Key Laboratory of Marine Materials and Protective Technologies, Ningbo Institute of Materials Technology and Engineering, Chinese Academy of Sciences, Ningbo 315201, China
[b] Ningbo Runner Industrial Corporation, Lingang Industrial Park, Xiangshan, Ningbo 315722, China

ABSTRACT

The present study is a part of continuing research efforts devoted to modifying nano titania by tailoring its structure for enhanced photocatalytic performances. The study concerns suspension plasma spray fabrication of black titanium dioxide coatings with porous microstructures and high photocatalytic activity. The black titania showed composite structure comprising anatase, rutile, metastable brookite, and $Ti_2O_3$ with markedly narrowed band gap of 2.71 eV. Further TEM characterization revealed that formation of the black titania was associated with grain growth and with tremendous lattice disorders, which are predominately responsible for visible light absorption. Examination of photocatalytic performances of the black titania coatings showed enhanced absorption and degradation of methylene blue under visible light, giving inspiring insights into surface coating construction of black titania for photocatalytic applications.

## 1. Introduction

A lot of pollutants existing in wastewater and air, for instance nutrients, organic matter and toxic metal ions produced from industries and daily life, introduced detrimental effects into the aquatic and air system due to their intensive colors and persistent toxicity [1–4]. Various methods have therefore been developed to tackle the pollution problems. Conventional treatment routes are usually based on biological and physical strategies, which in most cases brought about other concerns like generation of toxic secondary pollutants [5,6]. Extensive worldwide research efforts have therefore been devoted to developing new techniques, among which advanced oxidation processes (AOPs) were successful in eliminating organic compounds, pathogens and disinfection by-products by in situ generation of highly reactive transitory species and subsequent reactions [7–9]. As one of AOPs, heterogeneous photocatalysis employing semiconductor catalysts has been regarded as one of the most promising methods for its outstanding oxidative power and stability [10]. $TiO_2$ has drawn substantial attention as a semiconductor catalyst for cost efficiency, excellent thermal stability and mechanical properties [11]. It is noted, however, that the overall solar-driven photocatalytic efficiency of $TiO_2$ is predominately limited by its wide band gap working under UV illumination, which only accounts for ~5% in solar spectrum [9]. In addition, traditional techniques for fabricating bulk $TiO_2$ catalyst usually involve slurry processing,

consequently causing other undesired issues when the catalyst was separated from the mixture.

Many attempts in modifying the structure of nano titania, e.g. metal and non-metal doping [9], co-deposition of metals [12], and mixing of two semiconductors [13], have been made to accomplish visible light photo-response. Recently, it was realized that black titania has much better photocatalytic performances than other structures of titania, and several approaches have been explored to fabricate black titania [14]. Hydrogen thermal treatment with 20.0-bar pure $H_2$ atmosphere at 200 °C for 5 days was claimed successful in transforming white $TiO_2$ nanoparticles to black $TiO_2$ [15]. Hydrogen plasma treatment [16] and chemical reduction processing with the participation of aluminum [17], zinc [18], imidazole [19], $NaBH_4$ [20], and $CaH_2$ [21] were also reported for preparing black titania. Regardless of the extensive efforts made in recent years in making black titania, for example chemical oxidation [22], electrochemical reduction [23] and anodization-annealing [24], fabrication of black titania in the form of coating yet keeps elusive.

As a versatile surface coating technique, plasma spray is competitive in large-scale construction of nanostructured coatings [25–27]. In particular, liquid plasma spray has shown great promises in fabricating functional coatings using nanoparticles as starting feedstock [28]. Construction of nano titania coatings has been successful by suspension flame spray [29] and suspension plasma spray [30,31]. The structures
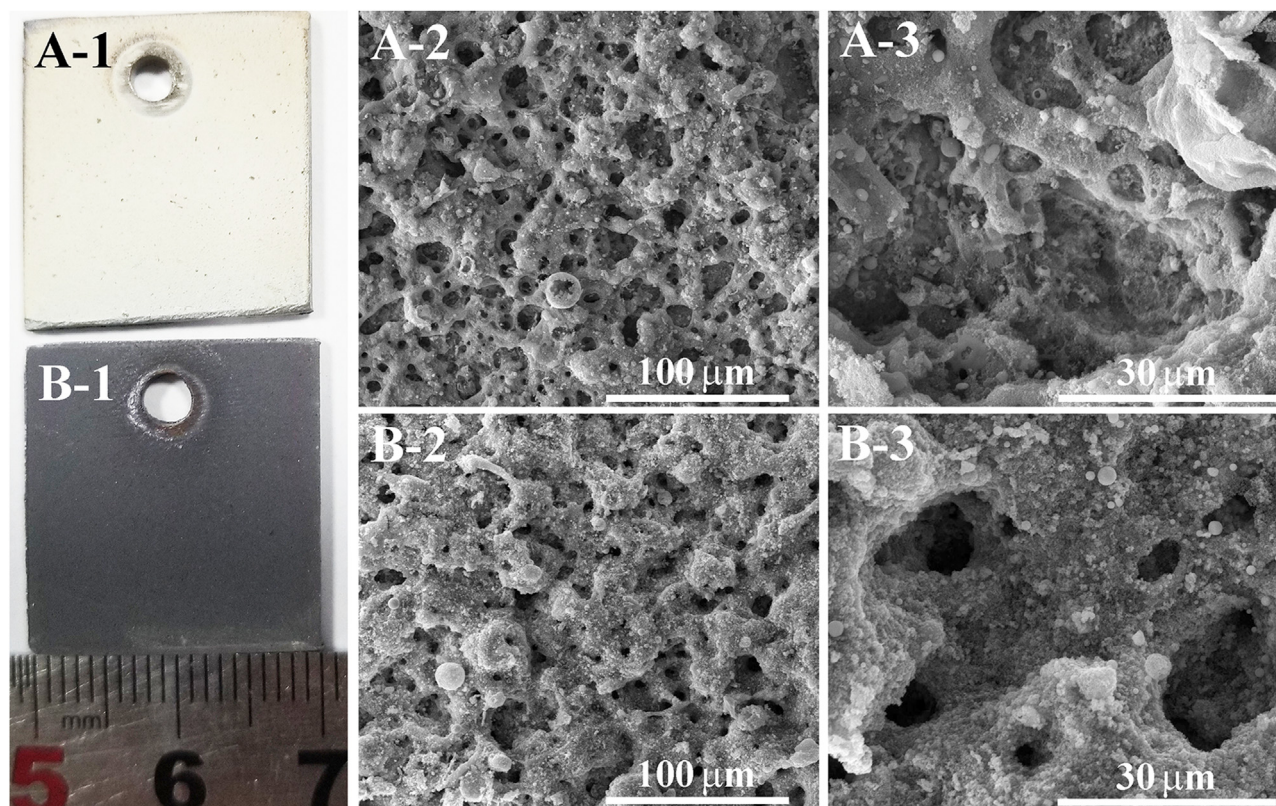
**Fig. 1.** Digital photos and topographical morphology of the white $TiO_2$ coating (A) and the black $TiO_2$ coating (B). (-3 is enlarged view of selected area in -2).
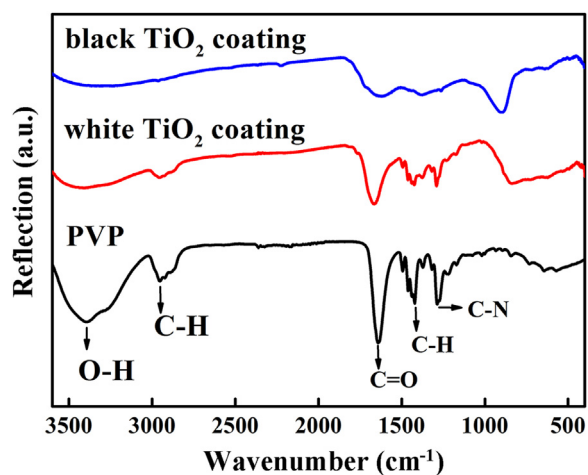


**Fig. 2.** FTIR spectra of the samples.

with porous zones containing fine nanometric and submicrometric grains were reported for the coatings [31]. During the spraying, liquid droplets usually facilitate acceleration of nanoparticles for subsequent impact coating formation, and evaporation of liquid alleviates effectively phase transformation of the nanomaterials at elevated temperatures [30]. In this work, suspension plasma spray was employed for making black $TiO_2$ coatings with controllable crystal phases through optimizing the spray parameters. Microstructural evolution of titania during the coating deposition and photocatalytic performances of the coatings were examined and elucidated.

## 2. Materials and methods

The suspension used for the coating deposition was prepared by dispersing 10 g Degussa $TiO_2$ (25 nm in diameter, Evonik Degussa P25, 99.5%) in 200 ml 50% ethanol solution after 3 g polyvinylpyrrolidone (PVP) and 0.5 g polyethylene glycol (PEG) were added. The mixing was carried out for 1 h under ultra-sonication and constant mechanical stirring. Coating deposition using the suspension was made using the APS-2000K plasma spray system (Beijing Aeronautical Manufacturing Technology Research Institute, China). During the spraying, the suspensions were fed into plasma torch through a home-made peristaltic pump equipped with a magnetic stirrer, and the flow rate was 90 ml/min. The spray distance was 80 mm, and the flow rate of Ar and $H_2$ was 15 ml/min and 1.8 ml/min, respectively. To attain the desired structure of the titania coatings, plasma spray power and gun moving speed were optimized and the robot-controlled moving speed was set within the range of 333–833 m/min. Sand-blasted 316 L stainless plates with the dimension of 20 mm × 20 mm × 2 mm were used as the substrates.

Microstructure of the coatings was characterized by field emission scanning electron microscopy (FESEM, FEI Quanta FEG250, the Netherlands). Chemical composition of the samples was further examined by Fourier transform infrared spectroscopy (FTIR, Nicolet 6700, Thermo Fisher Scientific, USA) with a resolution of $8 \, cm^{-1}$ and a scan number of 4 at the spectral region ranging from 400 to $3600 \, cm^{-1}$. Phase composition of the samples was detected by X-ray diffraction (XRD, Bruker AXS, Germany) at a scanning rate of 0.1°/s using Cu Ka radiation operated at 40 kV. UV–Visible diffuse reflectance spectra (UV–Vis DRS) of the coatings were recorded in the range of 200–800 nm with $BaSO_4$ being used as the reflectance reference. Further microstructure characterization was made using high resolution transmission electron microscopy (HRTEM, FEI Tecnai F20, the Netherlands). For the TEM sample preparation, the coatings were scrapped from substrates and then ultrasonic dispersion was carried out for 3 min. The suspension was then transferred onto copper micro-grids and the solvent evaporation was achieved with the aid of an infrared light.

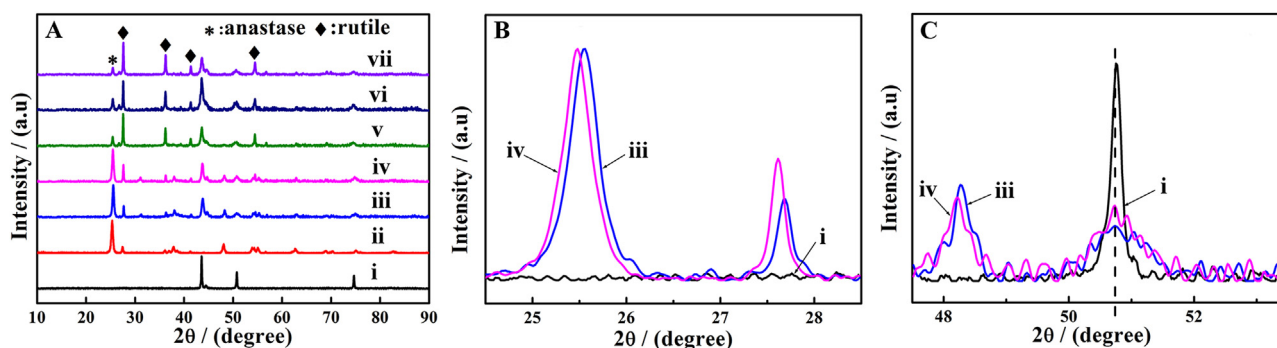Assessment of photocatalytic activity of the coatings was carried out

**Fig. 3.** XRD curves (A) of (i) the 316L substrate, (ii) the pristine P25 powder, (iii) the white $TiO_2$ coating (spray power of 30 kW and nozzle moving speed of 500 mm/s), and (iv-vii) the black $TiO_2$ coatings (iv: spray power of 30 kW and nozzle moving speed of 250 mm/s, v: spray power of 35 kW and nozzle moving speed of 250 mm/s, vi: spray power of 30 kW and nozzle moving speed of 200 mm/s, and vii: spray power of 36 kW and nozzle moving speed of 200 mm/s). Peak shifting is clearly seen from the spectra with 2theta ranges of 24.5–28.5° (B) and 47.75–52.75° (C).
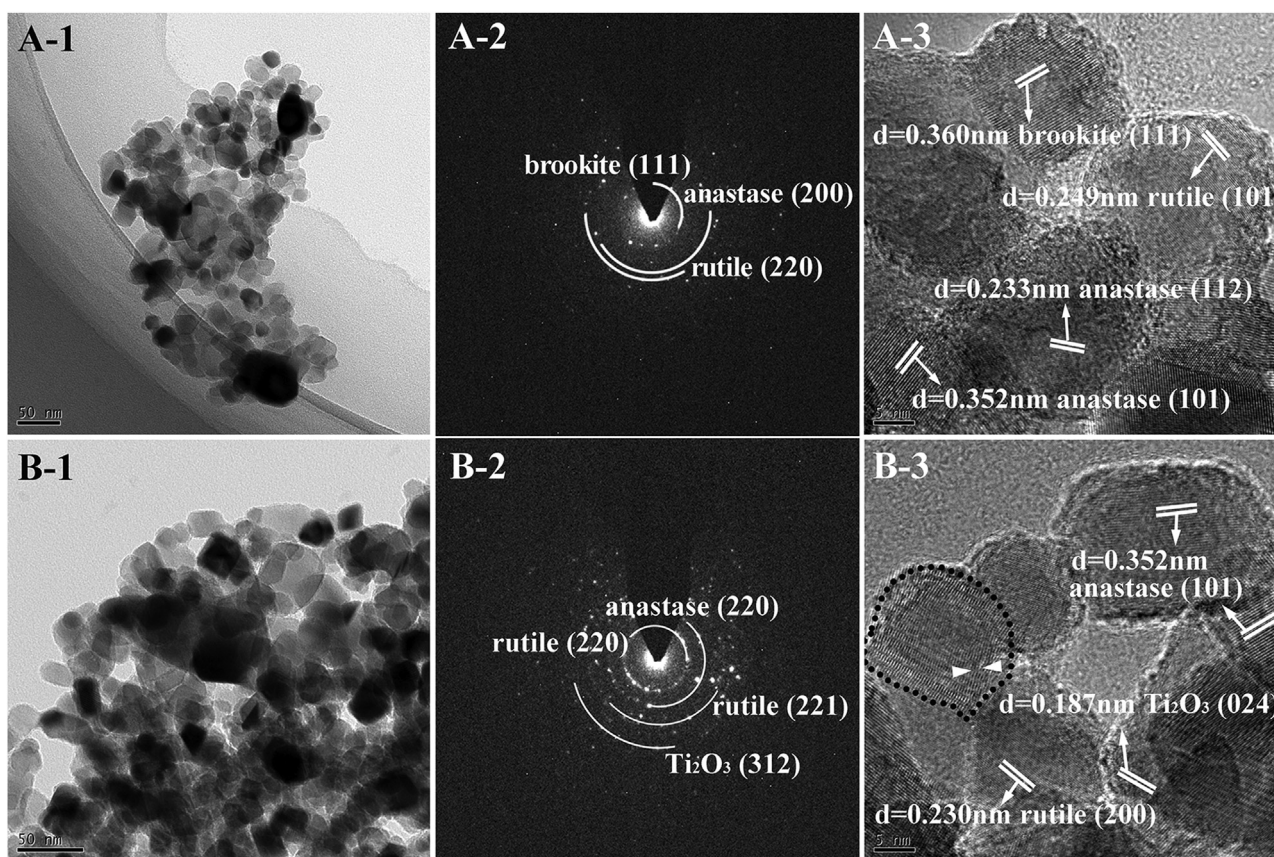


**Fig. 4.** TEM imaging analyses of the coatings, A-1: TEM image of the white $TiO_2$ coating, B-1: TEM image of the black $TiO_2$ coating, A-2: SAD pattern of the white $TiO_2$ coating, B-2: SAD pattern of the black $TiO_2$ coating, A-3: HRTEM micrograph of the white $TiO_2$ coating, B-3: HRTEM micrograph of the black $TiO_2$ coating.

by measuring the degradation of methyle blue (MB, Aladdin Reagent Corp., China) under both UV light (Philips, TL-D, 15 W) and Xe lamp (GXZ500). For the testing, the coating sample was immersed in a double-walled beaker which was positioned 15 cm below the lamp and was equipped with controllable circulating cooling water to eliminate thermal effect. After 15 ml MB solution (5 ppm) was added, the solution was magnetically stirred continuously. The whole testing system was subject to dark for 1 h to achieve a dye adsorption/desorption equilibrium prior to photo-irradiation. At every illumination interval, 1 h in this case, 0.5 ml suspension was taken out to determine the variation of MB concentration using a UV–vis spectrophotometer (MAPADA, UV-3300 spectrophotometer) by measuring the adsorption intensity at the absorbance wavelength of 664 nm.

## 3. Results and discussion

Optimization of operational spray parameters resulted in two distinguished colors of the coatings, white and black (Fig. 1). From the topographical views, it seems clear that both the coatings exhibited porous microstructure, which could be well explained by sudden decomposition of PVP in the spraying process. Once the atomized suspension was fed into the high temperature plasma torch, the decomposition usually resulted in formation of steam and gases. Release of the gases from the splats upon impingement on the substrate/pre-coating would easily result in formation of pores in the coatings, and these phenomena were already elucidated by Pravdic and Gani [32]. Higher plasma spray power would cause intensified expansion of the gases,
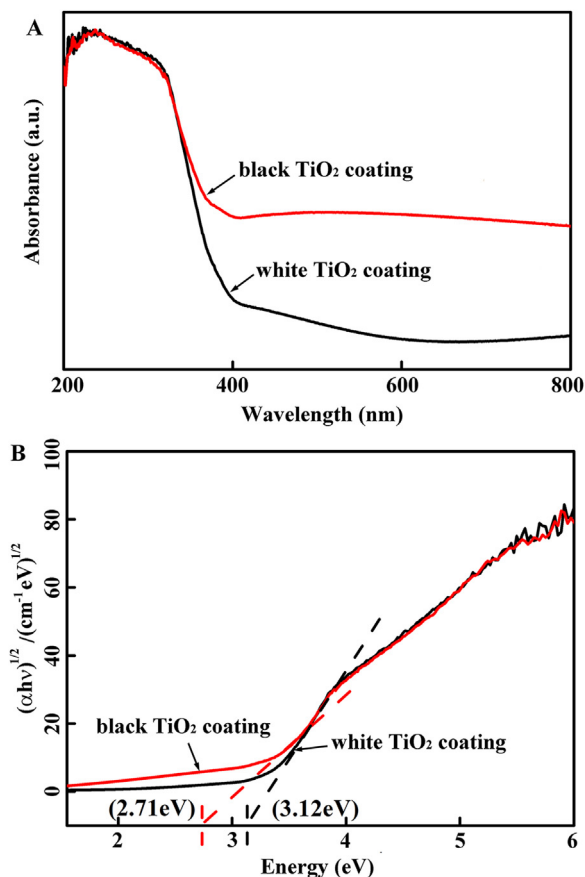
**Fig. 5.** Spectral absorbance (A) and Tauc plot (B) of the coatings.

which might explain the much larger pores seen from the topographical morphologies of the black coating than the white coating (Fig. 1B-3 vs. A-3). The black coating showed the open-pore sizes of up to 20 μm, while the white coating exhibited the pore sizes of less than 15 μm. This would in turn reflect different photocatalytic activity. Decomposition of PVP was further analyzed by FTIR (Fig. 2). The broad peak located at 3400 cm$^{-1}$ is attributed to water adsorbed on PVP surface and the carbonyl on pyrrolyl ring stretching vibration [33]. The peaks located at 2924–2843 cm$^{-1}$, 1671 cm$^{-1}$, 1462 cm$^{-1}$ and 1286 cm$^{-1}$ are assigned to C-H stretching vibrations, C==O stretching, -CH$_2$- stretching vibration, and C-N stretching vibration of PVP molecules, respectively [34–36]. The white TiO$_2$ coating showed the typical IR peaks referring to PVP at 2889 cm$^{-1}$, 1671 cm$^{-1}$, 1462 cm$^{-1}$ and 1286 cm$^{-1}$. These peaks suggest residual PVP in the white coating. The IR curve of the black coating showed much less content of PVP, only a shoulder peak at 1900–1260 cm$^{-1}$ is seen. Besides, the black coating showed the broad band located at 700–1000 cm$^{-1}$, referring to Ti-O and Ti-O-Ti skeletal frequency region [34]. These information is consistent with the spray parameters used for the coating deposition that the black coating was made using higher spray power. Disappearance by decomposition of PVP facilitates pore formation during the coating formation stage, which has already been seen in the SEM images.

In this study, the key plasma spray parameters were optimized predominantly by examining by XRD the phases of the as-sprayed coatings. It was noted that the spray power plays the key role in regulating the phase transformation of titania during coating formation stage (Fig. 3). Due to the small thickness of the coatings (less than 20 μm), the steel substrate was also detected. Anatase remained as the main phase in the white TiO$_2$ coating fabricated with the power of 30 kW and the gun moving speed of 500 mm/s (Fig. 3A-iii) and in the black TiO$_2$ coating fabricated with 30 kW power and the gun moving speed of 250 mm/s (Fig. 3A-iv). This is not surprising since liquid

evaporation occurred during the spraying could prevent the phase transformation of titania. The Magnelli phases that are usually seen in plasma sprayed titania coatings were hardly detected in this case. It is clear that increase in spray power or decrease in gun moving speed gives rise to decreased ratio of anatase to rutile, suggesting enhanced structure transformation of anatase to rutile. It is realized that as the power was higher than 30 kW or the gun moving speed was lowered down to less than 250 mm/s, the color of the coatings changed from white to black, indicating the presence of rutile (Fig. 3A-iii-vii). It should be noted that catalytic performance of anatase is more remarkable than that of rutile [37,38]. For this reason, developing the techniques for constructing photocatalytic titatia coatings must take into account significant existence of anatase phase. In this case, apart from the white coating, the black TiO$_2$ coating also showed the XRD peaks for anatase structure (Fig. 3). However, it is surprisingly noted that compared to the white coating, the black coating showed shifting of the peaks for anatase, 25.5–24.5° (Fig. 3B) and 48.2–48.1° (Fig. 3C), and peak shift was also seen for rutile phase (from 28.5° to 27.5°, Fig. 3B). As the reference peaks, those detected from the steel substrate did not show any shifting (Fig. 3C). The peak shifting of titania was believed to indicate presence of dissolved dopants lattice distortion [39], which would ultimately influence the photocatalytic performances.

Further TEM characterization revealed changes in lattice parameters of titania grains in the black coating (Fig. 4). The grains in the coatings showed similar morphology as the pristine P25 powder [40,41]. For both the coatings, close interconnection between adjacent grains was clearly seen, indicating favorable cohesion of the nanoparticles in the coatings. Transformation from anatase to rutile is associated with enlarged grain sizes [39], which can be clearly recognized from the TEM images in this study. The SAD patterns revealed the features of crystalline titania with the planes of (220), (101), (200) and (221) for rutile, (200), (112), (101), and (220) for anatase, and (111) for metastable brookite. Surprisingly, in the black titania coating, a more complex crystal phase with faint presence, Ti$_2$O$_3$ phase, was seen. In addition, the SAD pattern detected from the black coating showed apparently low angle grain boundary and moire fringes, which are generated by misalign [42,43]. The large number of lattice disorders would improve visible light absorption by bringing about band tail states and merging with the valance band. These states tend to become the center to guide optical excitation and relaxation. In addition, another advantage of the disorders in the black titania coating is their capability of potentially enhancing electron transfer and photocatalytic activity by providing trapping sites for photogenerated carriers and balancing their recombination speed [15,39,44]. It is probably the first time that the black titania structure was fabricated by thermal spraying, and the phase transformation of anatase (structure changes, grain growth, lattice disorder, etc.) is apparently tailored by the key spray variables.

Photocatalytic activity of the coatings was examined by acquiring their UV–vis diffuse reflectance spectra (Fig. 5). The black TiO$_2$ coating exhibited no difference in the absorption at UV-light region from the white coating, and an enhanced light adsorption occurred at the wavelengths between 360 and 800 nm. This presumably suggests that the black TiO$_2$ coating tends to absorb more visible light, showing much higher catalytic activity than the white coating. To study the changes in band gap of the coatings, Tacu plots were also acquired (Fig. 5b). As an indirect band gap semiconductor, TiO$_2$ has the photon energy (h$\nu$) on the abscissa and ($\alpha$h$\nu$)$^{1/2}$ on the ordinate of the Tacu plot, where $\alpha$ is the absorption coefficient of the semiconductor [45]. The band gaps are 2.71 eV and 3.12 eV for the black coating and the white coating, respectively, and the values were estimated by extrapolating the linear region to the abscissa, which was already proven reliable [46]. The results suggest greater ability of the black coating than the white coating to respond to the visible light wavelengths. The narrowed band gap, introduction of mid-gap states and improvement in charge carrier
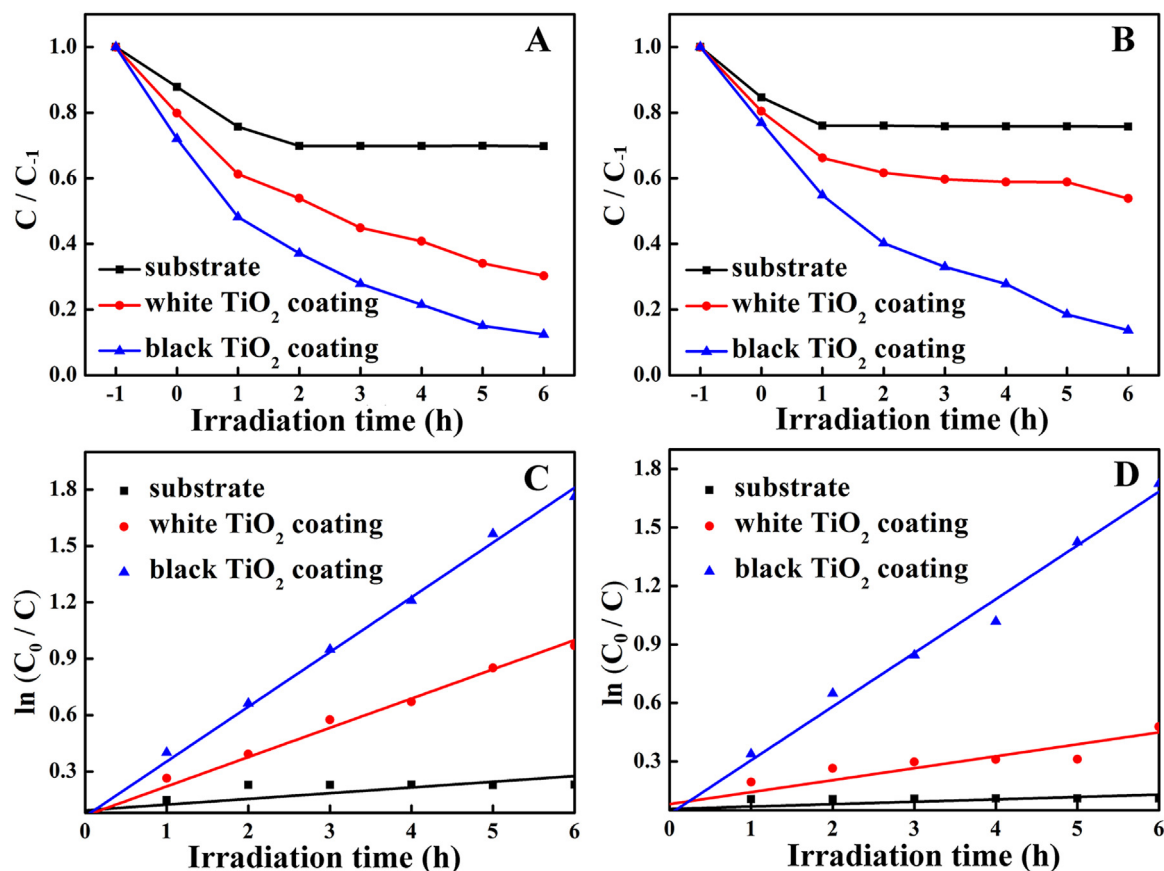
**Fig. 6.** Photocatalytic degradation of MB under UV light (A) and Xe lamp (B) irradiation, and linear transform ln ($C_0$/C) of the kinetic curves of MB degradation under the UV light (C) and Xe lamp (D) irradiation.

recombination induced by surface disorder of black titania could result in enhanced absorption in the visible light and near-infrared region [47,48]. In this case, the enhanced light response of the black titania coating is obviously attributed to the large amount of surface disorders that exist in the coating.

Photocatalytic activity of the coatings was further measured by degrading the dye MB under UV light and visible light irradiation sources (Fig. 6, $C_{-1}$ refers to the original concentration of MB in the solution). Due to strong absorption at the wavelengths shorter than 400 nm, the decolorization efficiency of MB under UV light is around ~ 91% for the black coating, ~ 18% more than that achieved by the white coating (Fig. 6A). As a comparison, MB degradation by the coatings and the substrate alone was also examined under Xe lamp illumination, which can produce visible wavelength light (Fig. 6B). Strikingly, MB degradation of ~ 89% under the visible light was achieved for the black TiO$_2$ coating, showing superior catalytic activity to the white coating and the substrate. Kinetics of photocatalytic degradation of low concentration organic pollutants by TiO$_2$ has been well established and can be described by Langmuir-Hinshelwood first-order kinetic model: ln $(\frac{C_0}{C})=k_{app} \times t$, where $C_O$ is the concentration of the dye after darkness adsorption, $C$ is the concentration of the dye measured at the time point $t$, and $k_{app}$ refers to the apparent rate constant [49]. The relationship between illumination time and degradation rate of the dye under UV and visible light illumination was plotted (Fig. 5C, D). The UV photocatalytic testing showed the apparent rate constant $k$ of 0.00056 min$^{-1}$, 0.00259 min$^{-1}$ and 0.004856 min$^{-1}$ for the substrate, the white TiO$_2$ coating and the black coating, respectively. In addition, the apparent rate constant $k$ of the control group, the white and the black samples examined under Xe lamp is 0.000204 min$^{-1}$, 0.001021 min$^{-1}$ and 0.004591 min$^{-1}$, respectively. It is therefore clear that the black titania coating possesses significantly enhanced

photocatalytic performances in particular under the visible light irradiation, which in turn gives insight into the appropriateness of plasma spray processing route for making structure disorders in titania for promoted photocatalytic activities.

## 4. Conclusions

Nanostructured titania coatings were fabricated by suspension plasma spraying, and the black TiO$_2$ structure was fabricated for the first time in titania coatings. The high temperature spray processing triggered partial structure transformations of anatase to rutile, brookite, and remarkable lattice disorders of anatase. The exceptional structure of the black titania coating gave rise to significantly enhanced photocatalytic activity under both UV and visible light irradiation, and the improvement in degrading MB under visible light irradiation is remarkable for the black coating. The results shed light on the efficient fabrication of photocatalytic titania coatings with tunable novel structures for enhanced performances.

## References

[1] J.M. Garrido, W.A.J. vanBenthum, M.C.M. vanLoosdrecht, J.J. Heijnen, Influence of

dissolved oxygen concentration on nitrite accumulation in a biofilm airlift suspension reactor, Biotechnol. Bioeng. 53 (1997) 168–178.

[2] C.A. Martinez-Huitle, E. Brillas, Decontamination of wastewaters containing synthetic organic dyes by electrochemical methods: a general review, Appl. Catal. B-Environ. 87 (2009) 105–145.

[3] T. Cai, S.Y. Park, Y. Li, Nutrient recovery from wastewater streams by microalgae: status and prospects, Renew. Sust. Energy Rev. 19 (2013) 360–369.

[4] M.C. Bordes, M. Vicent, R. Moreno, J. Garcia-Montano, A. Serra, E. Sanchez, Application of plasma-sprayed $TiO_2$ coatings for industrial (tannery) wastewater treatment, Ceram. Int. 41 (2015) 14468–14474.

[5] M.A. Barakat, New trends in removing heavy metals from industrial wastewater, Arab. J. Chem. 4 (2011) 361–377.

[6] K. Xu, G.M. Zeng, J.H. Huang, J.Y. Wu, Y.Y. Fang, G. Huang, H. Li, B. Xi, H. Liu, Removal of $Cd^{2+}$ from synthetic wastewater using micellar-enhanced ultrafiltration with hollow fiber membrane, Colloid Surf. A 294 (2007) 140–146.

[7] S. Esplugas, J. Gimenez, S. Contreras, E. Pascual, M. Rodriguez, Comparison of different advanced oxidation processes for phenol degradation, Water Res. 36 (2002) 1034–1042.

[8] M. Pera-Titus, V. Garcia-Molina, M.A. Banos, J. Gimenez, S. Esplugas, Degradation of chlorophenols by means of advanced oxidation processes: a general review, Appl. Catal. B-Environ. 47 (2004) 219–256.

[9] K. Wang, J. Yu, L. Liu, L. Hou, F. Jin, Hierarchical P-doped $TiO_2$ nanotubes array@Ti plate: towards advanced $CO_2$ photocatalytic reduction catalysts, Ceram. Int. 42 (2016) 16405–16411.

[10] U.I. Gaya, A.H. Abdullah, Heterogeneous photocatalytic degradation of organic contaminants over titanium dioxide: a review of fundamentals, progress and problems, J. Photochem. Photobiol. C 9 (2008) 1–12.

[11] A. Fujishima, K. Honda, Electrochemical photolysis of water at a aemiconductor electrode, Nature 238 (1972) 37–38.

[12] J.B. Park, J. Graciani, J. Evans, D. Stacchiola, S. Ma, P. Liu, A. Nambu, J. Fernandez Sanz, J. Hrbek, J.A. Rodriguez, High catalytic activity of $Au/CeO_x/TiO_2(110)$ controlled by the nature of the mixed-metal oxide at the nanometer level, Proc. Natl. Acad. Sci. USA 106 (2009) 4975–4980.

[13] X. Xu, G. Yang, J. Liang, S. Ding, C. Tang, H. Yang, W. Yan, G. Yang, D. Yu, Fabrication of one-dimensional heterostructured $TiO_2@SnO_2$ with enhanced photocatalytic activity, J. Mater. Chem. A 2 (2014) 116–122.

[14] X. Chen, L. Liu, F. Huang, Black titanium dioxide ($TiO_2$) nanomaterials, Chem. Soc. Rev. 44 (2015) 1861–1885.

[15] X. Chen, L. Liu, P.Y. Yu, S.S. Mao, Increasing solar absorption for photocatalysis with black hydrogenated titanium dioxide nanocrystals, Science 331 (2011) 746–750.

[16] G. Wang, H. Wang, Y. Ling, Y. Tang, X. Yang, R.C. Fitzmorris, C. Wang, J.Z. Zhang, Y. Li, Hydrogen-treated $TiO_2$ nanowire arrays for photoelectrochemical water splitting, Nano Lett. 11 (2011) 3026–3033.

[17] Z. Wang, C. Yang, T. Lin, H. Yin, P. Chen, D. Wan, F. Xu, F. Huang, J. Lin, X. Xie, M. Jiang, Visible-light photocatalytic, solar thermal and photoelectrochemical properties of aluminium-reduced black titania, Energy Environ. Sci. 6 (2013) 3007–3014.

[18] Z. Zhao, H. Tan, H. Zhao, Y. Lv, L.J. Zhou, Y. Song, Z. Sun, Reduced $TiO_2$ rutile nanorods with well-defined facets and their visible-light photocatalytic activity, Chem. Commun. 50 (2014) 2755–2757.

[19] X. Zou, J. Liu, J. Su, F. Zuo, J. Chen, P. Feng, Facile synthesis of thermal-and photostable titania with paramagnetic oxygen vacancies for visible-light photocatalysis, Chem.-Eur. J. 19 (2013) 2866–2873.

[20] Q. Kang, J. Cao, Y. Zhang, L. Liu, H. Xu, J. Ye, Reduced $TiO_2$ nanotube arrays for photoelectrochemical water splitting, J. Mater. Chem. A 1 (2013) 5766–5774.

[21] S. Tominaka, Topotactic reduction yielding black titanium oxide nanostructures as metallic electronic conductors, Inorg. Chem. 51 (2012) 10136–10140.

[22] X. Liu, S. Gao, H. Xu, Z. Lou, W. Wang, B. Huang, Y. Dai, Green synthetic approach for $Ti^{3+}$ self-doped $TiO_{2-x}$ nanoparticles with efficient visible light photocatalytic activity, Nanoscale 5 (2013) 1870–1875.

[23] C. Xu, Y. Song, L. Lu, C. Cheng, D. Liu, X. Fang, X. Chen, X. Zhu, D. Li, Electrochemically hydrogenated $TiO_2$ nanotubes with improved photoelectrochemical water splitting performance, Nanoscale Res. Lett. 8 (2013) 391.

[24] J. Dong, J. Han, Y. Liu, A. Nakajima, S. Matsushita, S. Wei, W. Gao, Defective black $TiO_2$ synthesized via anodization for visible-light photocatalysis, ACS Appl. Mater. Interfaces 6 (2014) 1385–1388.

[25] K. Ren, Y. Liu, X. He, H. Li, Suspension plasma spray fabrication of nanocrystalline titania hollow microspheres for photocatalytic applications, J. Therm. Spray. Technol. 24 (2015) 1213–1220.

[26] Q. Wu, J. Huang, H. Li, Deposition of porous nano-$WO_3$ coatings with tunable grain shapes by liquid plasma spraying for gas-sensing applications, Mater. Lett. 141 (2015) 100–103.

[27] L. Zhu, J. He, D. Yan, L. Xiao, Y. Dong, J. Zhang, H. Liao, Synthesis and microstructure observation of titanium carbonitride nanostructured coatings using reactive plasma spraying in atmosphere, Appl. Surf. Sci. 257 (2011) 8722–8727.

[28] X. Chen, B. Zhang, Y. Gong, P. Zhou, H. Li, Mechanical properties of nanodiamond-reinforced hydroxyapatite composite coatings deposited by suspension plasma spraying, Appl. Surf. Sci. 439 (2018) 60–65.

[29] Y. Liu, J. Huang, S. Ding, Y. Liu, J. Yuan, H. Li, Deposition, characterization, and enhanced adherence of Escherichia coli bacteria on flame-sprayed photocatalytic titania-hydroxyapatite coatings, J. Therm. Spray. Technol. 22 (2013) 1053–1062.

[30] F.L. Toma, G. Bertrand, S.O. Chwa, C. Meunier, D. Klein, C. Coddet, Comparative study on the photocatalytic decomposition of nitrogen oxides using $TiO_2$ coatings prepared by conventional plasma spraying and suspension plasma spraying, Surf. Coat. Technol. 200 (20–21) (2006) 5855–5862.

[31] S. Kozerski, F.L. Toma, L. Pawlowski, B. Leupolt, L. Latka, L.M. Berger, Suspension plasma sprayed $TiO_2$ coatings using different injectors and their photocatalytic properties, Surf. Coat. Technol. 205 (4) (2010) 980–986.

[32] G. Pravdic, M.S.J. Gani, The formation of hollow spherical ceramic oxide particles in a d.c. plasma, J. Mater. Sci. 31 (13) (1996) 3487–3495.

[33] X. Zhang, N. Sun, B. Wu, Y. Lu, T. Guan, W. Wu, Physical characterization of lansoprazole/PVP solid dispersion prepared by fluid-bed coating technique, Powder Technol. 182 (2008) 480–485.

[34] B. Rajamannan, S. Mugundan, G. Viruthagiri, P. Praveen, N. Shanmugam, Linear and nonlinear optical studies of bare and copper doped $TiO_2$ nanoparticles via sol gel technique, Spectrochim. Acta A 118 (2014) 651–656.

[35] A. Mahapatra, B.G. Mishra, G. Hota, Synthesis of ultra-fine alpha-$Al_2O_3$ fibers via electrospinning method, Ceram. Int. 37 (2011) 2329–2333.

[36] R. Topkaya, U. Kurtan, A. Baykal, M.S. Toprak, Polyvinylpyrrolidone (PVP)/$MnFe_2O_4$ nanocomposite: sol-gel autocombustion synthesis and its magnetic characterization, Ceram. Int. 39 (2013) 5651–5658.

[37] L.G. Devi, N. Kottam, S.G. Kumar, Preparation and characterization of Mn-doped titanates with a bicrystalline framework: correlation of the crystallite size with the synergistic effect on the photocatalytic activity, J. Phys. Chem. C 113 (2009) 15593–15601.

[38] T.T. Pham, N.H. Chinh, H.J. Lee, N.P. Thuy Duong, T.H. Son, C.K. Kim, E.W. Shin, Cu-doped $TiO_2$/reduced graphene oxide thin-film photocatalysts: effect of Cu content upon methylene blue removal in water, Ceram. Int. 41 (2015) 11184–11193.

[39] D.A.H. Hanaor, C.C. Sorrell, Review of the anatase to rutile phase transformation, J. Mater. Sci. 46 (2011) 855–874.

[40] F. Dong, H. Wang, Z. Wu, One-step "green" synthetic approach for mesoporous C-doped titanium dioxide with efficient visible light photocatalytic activity, J. Phys. Chem. C 113 (2009) 16717–16723.

[41] K.Y. Song, M.K. Park, Y.T. Kwon, H.W. Lee, W.J. Chung, W.I. Lee, Preparation of transparent particulate $MoO_3/TiO_2$ and $WO_3/TiO_2$ films and their photocatalytic properties, Chem. Mater. 13 (2001) 2349–2355.

[42] R.I. Bickley, T. Gonzalezcarreno, J.S. Lees, L. Palmisano, R.J.D. Tilley, A structural investigation of titanium-dioxide photocatalysis, J. Solid State Chem. 92 (1991) 178–190.

[43] R.L. Penn, J.F. Banfield, Imperfect oriented attachment: dislocation generation in defect-free nanocrystals, Science 281 (1998) 969–971.

[44] U. Diebold, The surface science of titanium dioxide, Surf. Sci. 48 (2003) 53–229.

[45] M.H. Habibi, M.H. Rahmati, Fabrication and characterization of ZnO@ CdS core–shell nanostructure using acetate precursors: XRD, FESEM, DRS, FTIR studies and effects of cadmium ion concentration on band gap, Spectrochim. Acta A 133 (2014) 13–18.

[46] S.I. Al-Mayman, M.S. Al-Johani, M.M. Mohamed, Y.S. Al-Zeghayer, S.M. Ramay, A.S. Al-Awadi, M.A. Soliman, $TiO_2$-ZnO photocatalysts synthesized by sol-gel auto-ignition technique for hydrogen production, Int. J. Hydrog. Energy 42 (2017) 5016–5025.

[47] A. Naldoni, M. Allieta, S. Santangelo, M. Marelli, F. Fabbri, S. Cappelli, C.L. Bianchi, R. Psaro, V. Dal Santo, Effect of nature and location of defects on bandgap narrowing in black $TiO_2$ nanoparticles, J. Am. Chem. Soc. 134 (2012) 7600–7603.

[48] X. Chen, L. Liu, Z. Liu, M.A. Marcus, W.C. Wang, N.A. Oyler, M.E. Grass, B. Mao, P.A. Glans, P.Y. Yu, J. Guo, S.S. Mao, Properties of disorder-engineered black titanium dioxide nanoparticles through hydrogenation, Sci. Rep. 3 (2013) 1510.

[49] Z. Hao, Z. Ruilong, Z. Jincai, Z. Yongfa, Dramatic visible photocatalytic degradation performances due to synergetic effect of $TiO_2$ with PANI, Environ. Sci. Technol. 42 (2008) 3803–3807.